sSynthesis and Surface Modification of Multi Walled Carbon Nanotubes as Electrode for Supercapacitor

Danlami Umar Zuru*, Bala Hassan*, Muhammad Nuraddeen Bui*, Aliyu Moh'd Mahuta*

*Department of Chemistry, School of Sciences, Adamu Augie College of Education, Argungu, Kebbi State, Nigeria
Corresponding Author: D. U. Zuru (Mobile phone: +2349067580036; E-mail address: duzuru2013@gmail.com)

Abstract— This work was an attempt to synthesize multi walled carbon nanotubes (MWCNTs) via chemical vapor deposition (CVD) method and chemically modify their surface wettability to enhance their energy storing capability. The as-grown sample was subjected to simple alkali/acid treatments, which results in the attachment of amide and carboxylic functional groups and the electrochemical analysis of the resulting electrode reveals about 290% pseudocapacitance contribution to the electrochemical double layer (EDL) capacitance in aqueous H_2SO_4 electrolyte. Highest specific capacitance of 86 F/g was recorded in aqueous KOH due to double layer capacitance only. Cyclic voltammograms of the sample reveals stable pseudocapacitive and S-shaped rectangular curves and the resulting charge/discharge profiles shows straight triangular lines. These outcomes may suggest possible application of these materials as potential electrode for both pseudocapacitor and electrochemical double layer capacitor (EDLC).

Index Terms— CVD, MWCNTs, surface wettability, functional groups, EDLC, pseudocapacitor

1 INTRODUCTION

The need for energy storage has necessitated intensive research in search of potential electrode materials for supercapacitor. Supercapacitors can store electric energy electrostatically via charge adsorption between the surface of a conductive electrode and an electrolyte, and through fast electron transfer which is achieved by redox reactions, the two types known as electrochemical double layer capacitors (EDLCs) and pseudocapacitors, respectively, [1]. Generally, higher capacitance was recorded for pseudocapacitors because the redox reactions can occur both on the surface and interior of the electrodes, while higher rate capability and satisfactory cycling life was observed for EDLCs [2]. Carbon nanotubes (CNTs) are attracting attention in the field of electronics as promising electrode materials for supercapacitor, because they possess good electrical conductivity and pore sizes suitable for storing electrolyte ions [3]. However, non-linearity of the specific surface area and pore size of CNTs with specific capacitance were also reported, which made it necessary to attribute capacitive contribution from other factors, such as attached oxygen containing functional groups (OFG) and nitrogen containing functional groups (NFG). Experimental observations have revealed that the influences of these moieties on the capacitance of CNTs have outweighed that of specific surface area. Attachment of functional groups on CNT matrix was observed to enhance their surface wettability which improves ion migration and greatly reduces the mass transfer resistance, making it easier to form electrochemical double layer (EDL) [4]. Reports on the specific capacitance of functionalized MWCNT electrodes tested in aqueous H_2SO_4 and KOH revealed pseudocapacitance and electrochemical double-layer capacitance, respectively, in their cyclic voltammograms (CVs). Specific capacitance (C_s) of 91 F/g, 104 F/g, 160 F/g and 68.8 F/g were reported of acid functionalized MWCNTs tested in H_2SO_4 electrolyte, while in aqueous KOH electrolyte, 80 F/g, 90 F/g, 140 F/g and 68 F/g were reported [5].

In the current report, MWCNTs are grown via chemical vapor deposition (CVD) pyrolysis of C_6H_{14}/N_2 feedstock on iron rich Fe_2O_3/Al_2O_3 catalyst. Chemical treatment is employed to attach OFG and NFG on the as-grown MWCNTs. The physico-chemical properties of the materials are analyzed using X-ray diffraction (XRD), field emission electron microscopy (FESEM) and high resolution transmission electron microscopy (HR-TEM). The attached functional groups are investigated using Fourier transformed infra-red (FT-IR) analysis and the electrochemical performance of the resulting MWCNT electrode tested in 1.0 M H_2SO_4 and 1.0 M KOH electrolytes.

2 MATERIALS AND METHODOLOGY

2.1 Catalyst Preparation

Appropriate amounts of $Fe(NO_3)_3.9H_2O$ and $Al(NO_3)_3.9H_2O$ (98%; Fisher) precursor salts were dissolved in 100 mL distilled water in a conical flask and stirred for 30 minutes, the resulting mixture was stirred for two hours, and left for another 24 hours, in order to achieve homogeneity. The nitrate solution was then dried for 48 hours at an adjusted temperature of 90•C. Calcination was performed in a Vulcan furnace at 450•C under air circulation for two hours, at a heating rate of 5•C/min. to obtain the desired Fe_2O_3/Al_2O_3 catalyst matrix.

2.2. CNT Synthesis

A split type horizontal furnace (LT Furnace STF-30-1200 model) was used in the pyrolysis of C_6H_{14}/N_2 feedstock on the Fe_2O_3/Al_2O_3 catalyst matrix at 850°C, under nitrogen gas flow rate of 100 mL/min. About 1.0 gram of the catalyst powder was loaded in an alumina boat and the pyrolysis time was set for 60 min. at 0.06 mL/min., resulting products were then cooled and scraped into sample bottles until required.

2.3. CNT Acid Treatment

The alkali-acid treatment employed is in accordance with the report of Weng et al [6]. About 50 mg of the as-grown MWCNTs sample is mixed with 40 mL of 4 M NaOH solution at 50°C and stirred with a magnetic stirrer for two hours. Aluminum complex precipitate is formed and removed by decantation and resulting residues batched washed with distilled water via centrifugation, until the solution is clear. Resulting solid MWCNT sample is then dried and dissolved in a mixture of concentrated H_2SO_4/HNO_3 solution (3:1) ratio, ultrasonicated for one hour at 60°C; batch washed with distilled water via centrifugation to obtain a neutral solution. The solid content is finally dried for four hours at 150°C and stored in sample bottles until required.

2.4. Catalyst and MWNT Characterization

The X-ray diffraction patterns of the prepared catalyst was obtained using an X-RD-6000 powder diffract meter of CuK_α radiation (λ = 0.15406 Å) operated at 40 kV and 30 mA at 4°C min^{-1}. Morphology of the sample MWCNTs was analyzed using a field-emission-scanning electron microscope (FESEM) (FEI Nova Nanosem 230), operated at 15 kV and a Zeiss EM 902A high resolution transmission electron microscope. Attached functional groups were investigated using Fourier transformed infra-red analysis. An Auto lab PGSTAT204/FRA32M module was used in the electrochemical analysis, using a three-electrode cell. The working electrodes consisted of treated MWCNTs coated on a glassy carbon electrode (GCE) and were tested in 1.0 M H_2SO_4 and 1.0 M KOH electrolytes. Pt. wire and Ag/AgCl/saturated served as counter and reference electrodes, respectively. In preparing the CNT electrode, about 10 mg of powdered CNTs was dispersed in 10 mL of distilled water and sonicated for 15 min. in an ultrasonic bath, to obtain a stable suspension. About 5 µL of the suspension was drop casted on a bare glassy carbon electrode (GCE), using a micropipette and the MWCNT-GCE electrodes were left to dry at room temperature. Cyclic voltammetry tests were conducted at scan rates of 0.01 Vs^{-1}, 0.02 Vs^{-1}, 0.03 Vs^{-1}, 0.05 Vs^{-1}, 0.1 Vs^{-1} and 0.2 Vs^{-1}; potential windows were set from 0.0 V to 1.0 V, and 0.3 V to 1.0 V in the aqueous 1.0 M H_2SO_4 solution, while -0.2 V to 0.6 V was set in aqueous KOH solution. Charge-discharge tests were set at around 1.0E-5 V to -1.0E-5 V. Quantitative evaluation of the charge storage ability of the MWCNTs were determined by the electrode mass (m), potential window (ΔE) and the voltammetry charges (Q), from which the specific capacitance (C_s) were calculated using equation 1.

$$C_s = \frac{Q}{\Delta E \times m} \quad (1)$$

The voltammetry charge (Q) was estimated from the sum of the anodic and cathodic charges, by dividing the integral area of the CV curve (A) with the CV scan rate [7], using an OriginPro 9.0 64 Bit. Software.

3. RESULTS AND DISCUSSION

3.1 Physico-chemical Analyses of Catalyst

X-RD analysis of the sample catalyst revealed diffraction peaks at 2Θ = 24.3°, 33.2°, 35.6°, 41.1°, 49.6°, 54.2°, 62.6° and 64.2°, which were attributed to (012), (104), (110), (113), (024), (116), (214) and (300) reflections of hematite iron oxide, α-Fe_2O_3, respectively, (JCPD no. 03-0664) [8], as shown in Figure 1. This result shows that the Al_2O_3 phase was incorporated into the crystal phases of Fe_2O_3 at 450°C, as evidenced by the broadening of the XRD reflections.

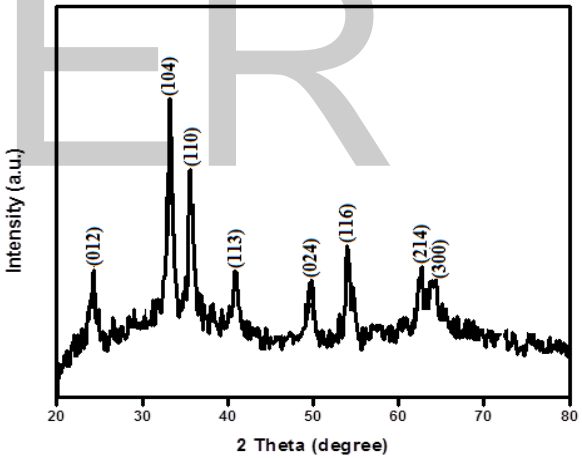

Figure 1: X-RD profile of as-prepared Fe_2O_3/Al_2O_3 catalyst showing different phases of α-Fe_2O_3 in which Al_2O_3 was incorporated.

The FESEM image of the catalyst sample in Figure 2 revealed nanometer sized pellet of particles with few larger agglomerations and the resulting EDS elemental analysis (inset) indicated the presence of only the original elements (O, Al and Fe) in the sample, suggesting high crystalline purity [9].

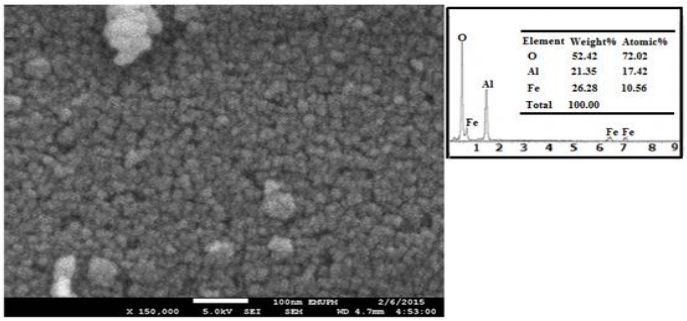

Figure 2: FESEM image of the Fe_2O_3/Al_2O_3 catalyst matrix showing nanosized pellet particles, inset was the resulting EDS profile showing the original O, Al and Fe elements.

3.2 Physico-chemical Analysis of MWCNTs

The XRD profile of the as-grown MWCNTs was displayed in Figure 3, in which the 2Θ (degree) diffraction peaks at approximately, 26.6 was attributed to hexagonal C (002) (JCPDS file no. 75 – 1621); α-Fe_2O_3 reflections occur at 35.3, 45.2, and 49.3 in the (200), (332) and (024) phases, respectively, [10]. The peaks appearing at 37.8 and 43.0-43.9 are reflections of γ''-FeN in the (111) and (200) directions, respectively, [11]. Peaks at 39.9, 40.8 and 48.8 were patterns of Fe_3C in the (002), (201) and (200) phases, respectively, (JCPDS file no. 34 – 1), and the strong peak at 44.8 was attributed to α-Fe (110)/Fe_3C (220) overlap (JCPDS file no. 6 – 696) [12]. Reflections of α-Al_2O_3 appeared at 46.0 and 66.7 in the (221) and (440) directions (ICDD file no. 10 - 0425) [13] while diffraction at 65.1 was a reflection of α-Fe (200) and agreed with (JCPDS file no. 6 – 696) [12]. The appearance of γ''-FeN and Fe_3C moieties was in agreement with the spin density functional theory, which revealed that both nitrogen and carbon atoms can occupy tetrahedral sites in the close-packing structure of Fe lattices via strong p-d covalent bonding, and stability of the composites were sustained through charge transfer to nitrogen and carbon atoms. Their appearance was also an indication that the MWCNT growth occurred on surface of the reduced catalyst, and the N, C and H atoms might have been generated by the decomposition of C_6H_{14}/N_2 feedstock on the Fe_2O_3/Al_2O_3 catalyst matrix during CVD pyrolysis [14].

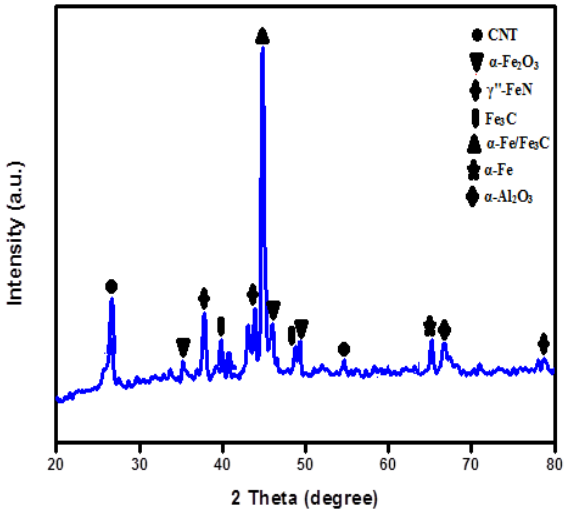

Figure 3: X-RD patterns of the as-grown MWCNTs showing presence of carbides and nitrides, suggesting that growth occurred on elemental metals.

The FESEM and TEM images of the as-grown MWCNTs sample were displayed in Figure 4 (a) and (b), respectively. The external morphology of the materials showed highly dense and entangled network of MWCNTs (Figure 4a), while the internal morphology revealed high purity image (Figure 4b).

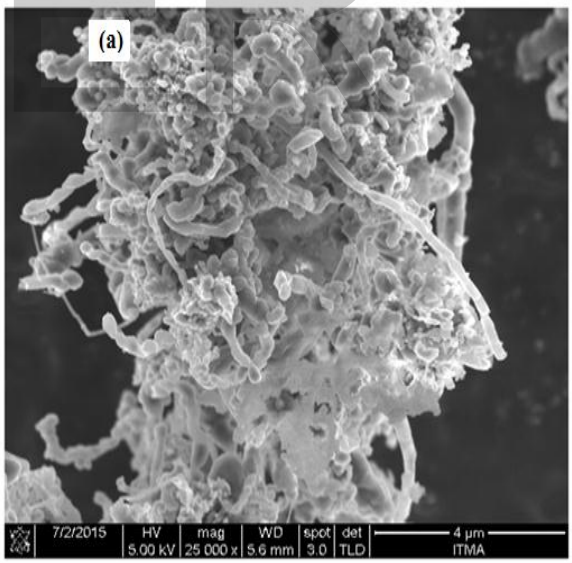

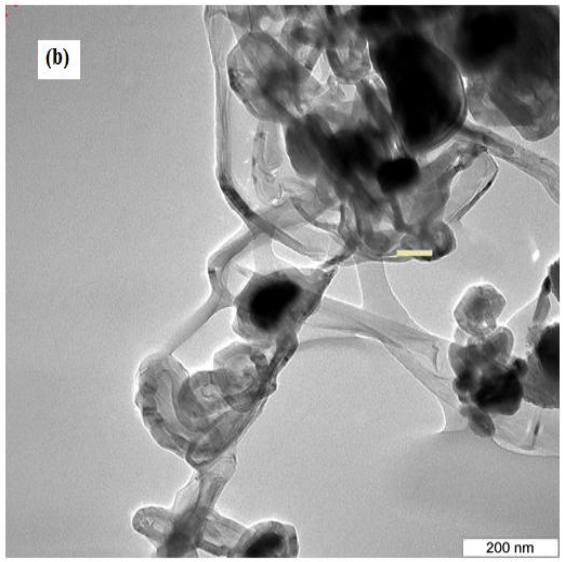

Figure 4: (a) FESEM image of the MWCNTs showing entangled network (b) TEM image showing high purity internal morphology.

High resolution transmission electron microscopy analysis of the samples also revealed long tubes of high purity MWCNT image, as shown in Figure 5a, while 5b revealed stacking of the graphene basal planes parallel to the tube axis, one carbon thick (0.33 nm).

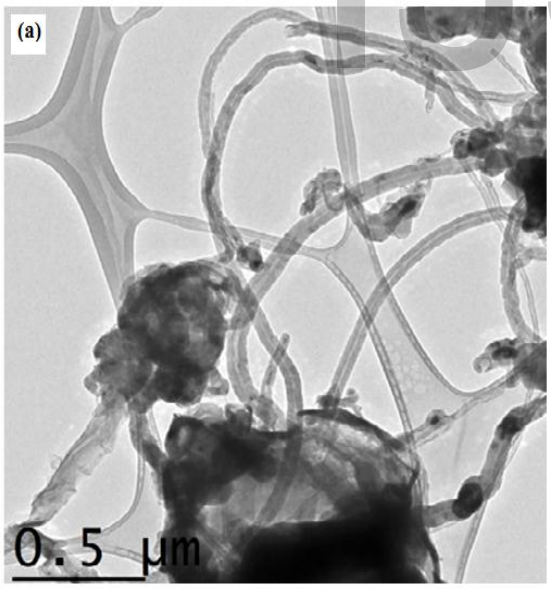

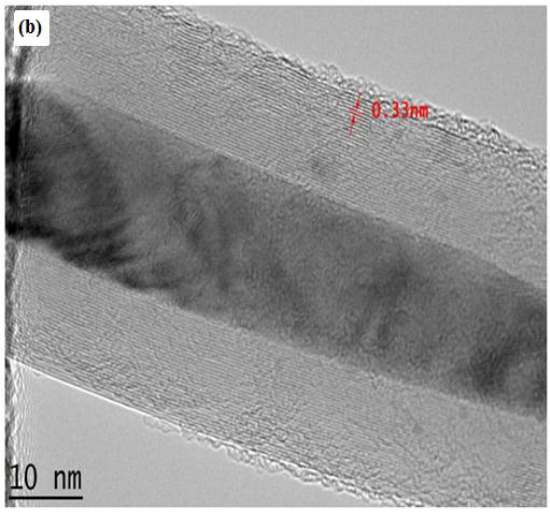

Figure 5: (a) HR-TEM images showing long tubes of high purity (b) HR-TEM images showing an enlarged MWCNT with stacking of the tube axis 0.33 nm thick.

The Raman profile of the as-grown MWCNTs showed weak D-band at 1351 cm^{-1}, and a strong G-band peak at 1582 cm^{-1} with resulting ID/IG ratio of 0.2, suggesting high graphitization or low impurities in the sample.

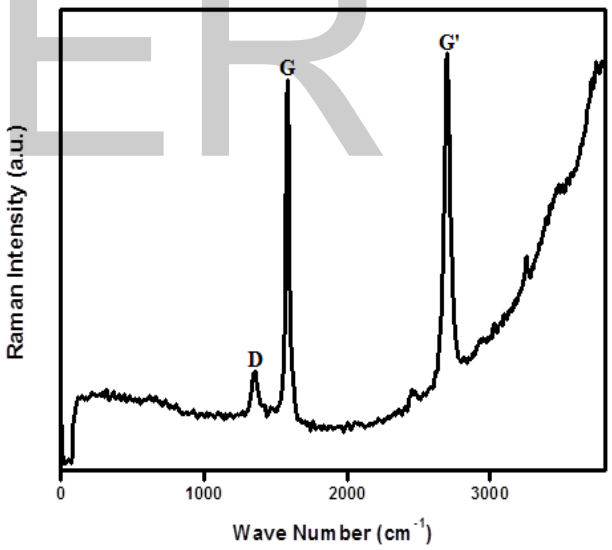

Figure 6: Plot of Raman profile of the synthesized MWCNTs showing important features, absence of RBM peak confirmed them multi walled.

The G'-band peak at 2697 cm^{-1} was an indication of high degree of long range order in the sample [15]. Another interesting observation was the weak peak appearing at 2472cm^{-1}, which suggested good quality experimental control [16].
The HR-TEM image of the treated MWCNT sample and the resulting FT-IR profile are shown in Figure 7 (a) and (b), respectively. Image of the treated sample indicated broken and defected tubes, which may suggest presence of attached

functional groups, as confirmed by their FT-IR profile. In the FT-IR profile, peaks appearing in the range 1600 cm^{-1} – 1699 cm^{-1} correspond to stretching vibration from amide carbonyl functional group (-C=ONHR) [17] and reflection from 1000 cm^{-1} to 1300 cm^{-1} was attributed to a bending vibration from -COOH moiety.

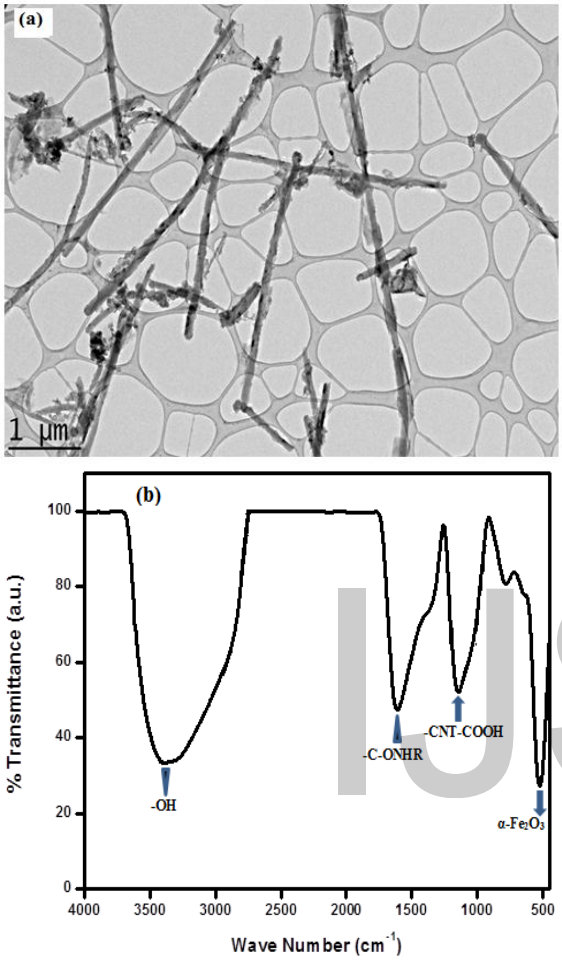

Figure 7: (a) HR-TEM image of MWCNTs after treatments showing broken tubes and side defects (b) FT-IR profile of the acid/alkali treated MWCNTs showing attached OFG and NFG.

The O-H stretching vibration appeared at 3060 cm^{-1} - 3744 cm^{-1} due to ambient atmospheric moisture or oxidation [18]. Peak reflection in the range 500 cm^{-1}-850 cm^{-1} was attributed to α-Fe oxide phase [19]. This result was an indication that oxygen containing functional group and nitrogen functional group were successfully attached on the surface of the MWCNTs. It was observed that the O and N atoms in the functional groups may both act as electron donors when they interact with the CNT matrix, using their available electrons in the formation of delocalized π-bonds with the adjacent carbon atoms of CNTs [20]. The functional groups were known to enhance the electrochemical properties of CNTs via surface wettability.

3.3 Electrochemical Analysis of the CNT Electrode

Table 1 was the recorded specific capacitance of the sample CNTs estimated from the integral area of the CV curve and the charge at different scan rates, in acidic and alkaline electrolytes.

TABLE 1

SPECIFIC CAPACITANCE OF ACID/ALKALI TREATED MWCNTS TESTED (A) FROM 0.0 V – 1.0 V, (B) FROM 0.3 V - 1.0 V IN 1.0 M H_2SO_4 AND IN 1.0 M KOH FROM -0.2 V TO 1.0 V.

Scan Rate (V/s)	Specific Capacitance (F/g)		
	1.0 M H_2SO_4 (a)	1.0 M H_2SO_4 (b)	1.0 M KOH
0.01	173	32	71
0.02	157	35	78
0.03	150	39	83
0.05	140	36	86
0.1	126	38	86
0.2	110	38	84

In 1.0 M H_2SO_4 (a) the potential window was opened from 0.0 V to 1.0 V in which the highest C_s. of 173 F g^{-1} was obtained at the lowest scan rate of 0.01 V s^{-1}, and a low capacitance of 44 F g^{-1} at 0.03 V s^{-1} was obtained when the potential window was reduced to 0.3 V – 1.0 V, where only electrochemical double layer (EDL) capacitance was suspected, as recorded in 1.0 M H_2SO_4 (b). Outcome of this analysis indicated about four times (293%) increase in the C_s., due to pseudocapacitance contribution of the OFG and NFG moieties. However, the specific capacitance was observed to decrease with increasing scan rate, which was attributed to degradation of the functional groups in the acidic medium. In H_2SO_4 (b), the specific capacitance showed a fluctuation decrease at 0.02 V s^{-1} and 0.05 V s^{-1} scan rates, suggesting either a decrease in the concentration of H^+ ions or the electrode might have moved slightly due to increase in current. In 1.0 M KOH electrolyte the C_s. recorded for the MWCNT electrode was 86 F/g at scan rates of 0.05 V s^{-1} and 0.1 V s^{-1} which is about twice the value obtained in the 1.0 M H_2SO_4 (b). These results indicated that although high C_s. was recorded in H_2SO_4 (a) in Table 1, due to pseudocapacitive contribution, however smooth electrode-electrolyte interaction were observed in the EDL of H_2SO_4 (b) and 1.0 M KOH, as their C_s. increases fairly with increase in scan rate.

Figure 8 were CV plots of the functionalized MWCNT sample, tested in 1.0 M H_2SO_4 from 0.0 V to 1.0 V and 0.3 V to 1.0 V represented in (a) and (b), respectively. CV curve of the same sample tested in 1.0 M KOH from -0.2 V to 0.5 V was displayed in Figure 8 (c). All the CVs revealed increase in current-potential response in conformity with Rondles-Sevcik law. The CV curve of the sample in Figure 8 (a) showed enhanced current-potential responses with pseudo-

capacitive behavior, indicating high power and possible application for pseudocapacitor [7]. The essence of pseudocapacitance observed in 1.0 M H_2SO_4 (a) may be due to the fact that, in this medium, the functionalized MWCNT electrode forms the negatively charged cathode which was surrounded by the hydronium ions (H_3O^+) of the acid.

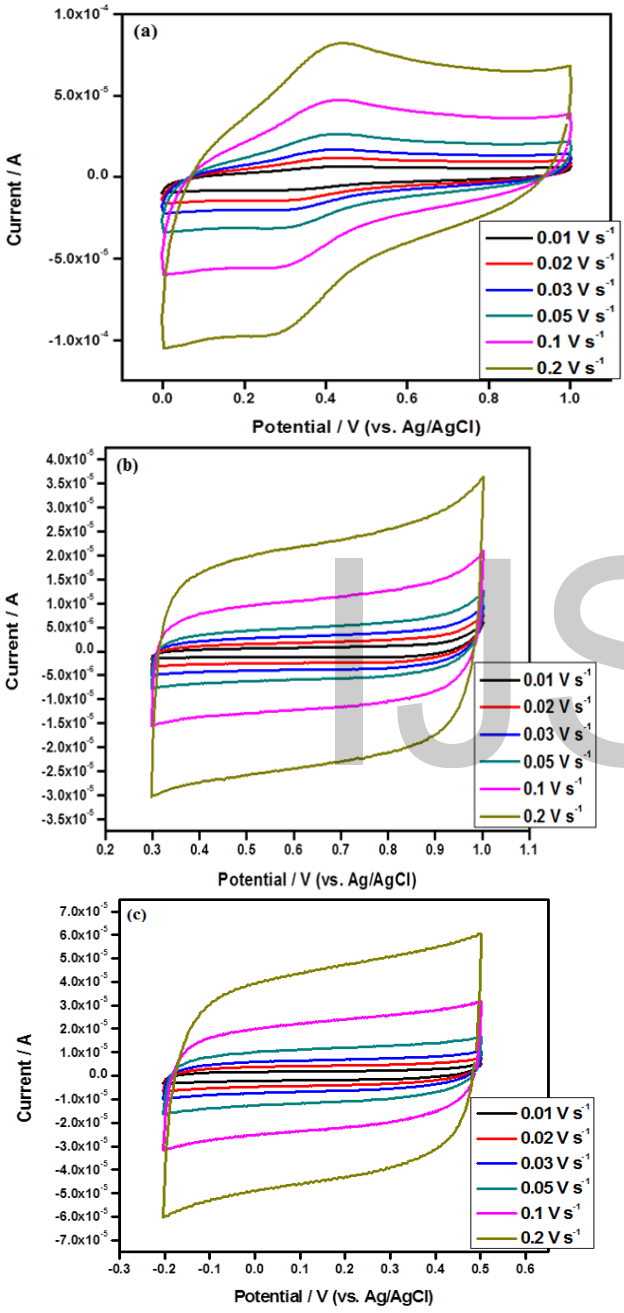

Figure 8: (a) Plot of cyclic voltammograms of the treated MWCNT electrode tested in 0.1 M H_2SO_4 in the 0.0 - 1.0 V potential windows (b) Plot of cyclic voltammograms of the treated MWCNT electrode tested in 0.1 M H_2SO_4 0.3 - 1.0 V potential windows (c) Plot of cyclic voltammograms of the treated MWCNT electrode tested in 1.0 M KOH in the -0.2 – 0.5 V potential windows.

When a strong electric field is applied, the bond lengths and bond angles of functional groups on CNT surface and H_3O^+ will be reduced, bringing the two molecules closer to each other, such that their electron clouds interact. Consequently, electrons may be shifted from the functional group to the O atom of the H_3O^+, making it a negatively charged center [21]. Figures 8 (b) and (c) showed stable rectangular S-shaped curves typical of an EDL up to scan rate of 200 mV/s, suggesting suitable potential as electrode for EDLC [22]. In aqueous alkaline KOH electrolyte, the small size and large polarization intensity of K^+ (3.31 Å) hydrated ions was reported to facilitates high charge density of an EDL. The absence of visible redox peak in the resulting CV was because the attached function groups might have inhibited the migration of the hydrated K^+ into the pores of the CNT, forcing them to diffuse into the bulk solution of the EDL. This was responsible for the S-shaped CV, in which K^+ ions were observed to form an inner Helmholtz layer (IHP) with electrode surface at low potential. In the middle potential, the interfacial tension reached maximum, dispersing the K^+ ions as the functional groups channel their diffusion into the bulk EDL solution due to steric hindrance which results in low capacitance. At high potential, the K^+ are then squeezed giving rise to insertion/deinsertion reactions in the pores of electrode which generate additional capacitive contribution [23].

Resulting plots of charge/discharge curves for the MWCNT electrode in the acidic and alkaline media were represented in Figure 9 (a) and (b), respectively. The profiles revealed stable triangular straight lines and the corresponding charge/discharge occurred in about of 60 seconds in 1.0 M H_2SO_4 and 45 seconds in 1.0 M KOH, which was also a suggestion that the materials may be suitable as supercapacitor electrode [7].

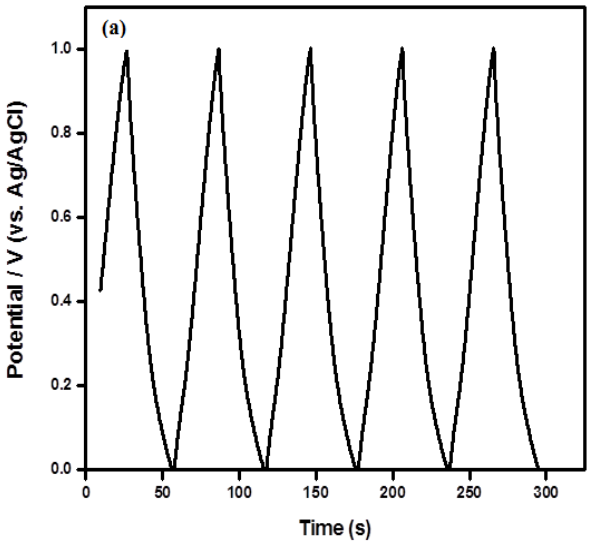

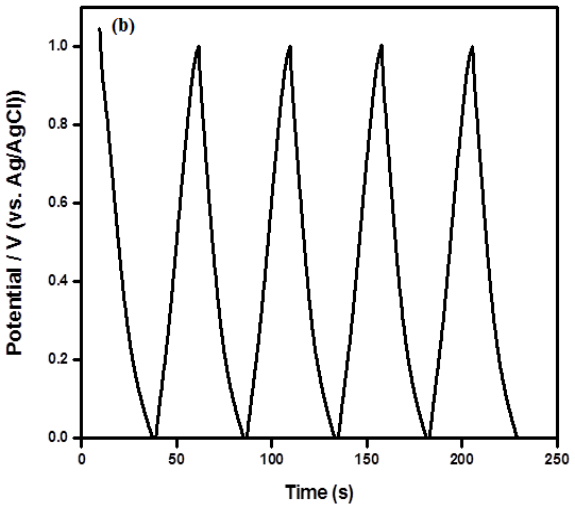

Figure 9: (a) Plot of charge/discharge curves for MWCNT electrode tested in 1.0 M H_2SO_4 showing estimated 60 seconds duration (b) Plot of charge/discharge curves for MWCNT electrode tested 1.0 M KOH, showing estimated 45 seconds duration.

4. CONCLUSION

Introduction of functional groups results in about 293% increase in the specific capacitance of the MWCNT electrode tested in 1.0 M H_2SO_4 electrolyte from 0.0 V to 1.0 V potential window. Stable rectangular S-shaped EDL CVs were obtained from 0.3 V to 1.0 V in 1.0 M H_2SO_4 and from -0.2 V to 0.5 V in 1.0 M KOH suggesting smooth electrode-electrolyte interactions, as their C_s. fairly increases with increasing scan rate. The electrode also showed straight triangular charge-discharge curves in both electrolytes. These observations may suggest that the functionalized MWCNTs may be potential electrode materials for electrical double layer capacitor in 1.0 M KOH and for pseudocapacitor in 1.0 M H_2SO_4.

ACKNOWLEDGEMENTS

The funding by the Adamu Augie College of Education, Kebbi-State, Nigeria, is hereby acknowledged and appreciated; however, all ideas contained in this manuscript reflect the decision of the authors alone.

REFERENCES

[1] Conway, B. E (1999). Electrochemical Supercapacitors Scientific Fundamentals and Technological Applications. Berlin Springer, ISBN 0306457369.

[2] Zhong, Y., Xia, X., Shi, F., Zhan, J., Tu, J and Fan, H. J (2016). Transition metal carbides and nitrides in energy storage and conversion. *Adv. Sci.* **3**. DOI: 10.1002/advs.

[3] Azam, M. A., Fujiwara, A and Shimoda, T (2013). Significant Capacitance Performance of Vertically Aligned Single-walled Carbon Nanotube Supercapacitor by Varying Potassium Hydroxide Concentration. *Int. J. Electrochem. Sci*. **8**, 3902 – 3911.

[4] Lozano-Castello, D., Cazorla- Amoros, D., Linares-Solano, A., Shirashi, S., Kurihara, H and Oya, A (2003). Influence of pore structure and surface chemistry on electric double layer capacitance in non-aqueous electrolyte. *Carbon*. **41**, 1765-1775.

[5] Gu, W and Yushin, G (2013). Review of nanostructured carbon materials for electrochemical capacitor applications: advantages and limitations of activated carbon, carbide-derived carbon, zeolite-templated carbon, carbon aerogels, carbon nanotubes, onion-like carbon, and graphene. *WIREs Energy Environ*. Doi: 10.1002/wene.102.

[6] Weng, Z., Liu, W., Yin, L-C., Fang, R., Li, M., Altman, E. I., Fan, Q., Li, F., Cheng, H-M. and Wang, H (2015). Metal/oxide interface nano-structures generated by surface segregation for electrocatalysis. *Nano Lett.* **15** (11), 7704-7710.

[7] Zhong, C., Deng, Y., Qiao, J, Hu, W., Zhang, L and Zhang, J (2015). A review of electrolyte materials and compositions for electrochemical supercapacitors. *Chem. Soc. Rev.* **44** (**21**), 7484-7920.

[8] Liu, p., He, S., Wei, H., Wang, J and Sun, C (2015). Characterization of α-Fe_2O_3/γ-Al_2O_3 Catalysts for Catalytic Wet Peroxide Oxidation of *m*-Cresol. *Ind. Eng. Res*. **54**, 130 – 136.

[9] Gulshan, F and Okada, K (2013).Preparation of Alumina-Iron Oxide Compounds by Co-precipitation Method and its characterization. *American Journal of Material Sciences and Engineering*. **1** (**1**), 6 – 11.

[10] Kumar, B. V., Thomas, R., Mathew, A., Rao, G. M., Mangalaraj, D., Ponpandian, N and Viswanathan C (2014). Effect of catalyst concentration on the synthesis of MWCNT by single step pyrolysis. *Adv. Mat. Lett*. **5** (**9**), 543 – 548.

[11] Wang, X., Zheng, W. T., Tien, H. W., Yu, S. S., Zu, W., Meng, S. H., He, X. D., Han, J. C., Sun, C. Q and Tay, B. K (2003). Growth, structural and magnetic properties of Iron nitride thin films deposited by dc magnetic sputtering. *Applied Surface Science.* **220**, 30 – 39.

[12] Krisyuk, V., Gleizes, A. N., Aloui, L., Turgambaeva, A., Sarapata, B., Prud, H. N., Senocq, F., Samelor, D., Zielinska-Lipiec, A., deCaro, D and Vahlas, C (2010). Chemical Vapour Decomposition of Iron, Iron Carbides and Iron Nitride Films from Amidinate Precursors. Journal of the Electrochemical Society (JES). **157** (**8**), D454 – D461.

[13] Santos, P. S., Santos, H. S and Toledo, S. P (2000). Standard Transition Aluminas. Electron Microscopy Studies. Materials Research, **3** (**4**), 104 – 114.

[14] Yang, F., Wang, X., Zhang, D., Yang, J., Luo, D., Xu, Z., Wei, J., Wang, J-Q., Xu, Z., Peng, F., Li, X., Li, R., Li, M.,

Bai, X., Ding, F and Li, Y (2014). Chirality-specific growth of single-walled carbon nanotubes on solid alloy catalysts. *Nature Lett.* **510**, 522-532.

[15] Lehman, J. H., Terrones, M., Mansfield, E., Hurst, K. E and Meunier, V (2011). Evaluating the characteristics of multiwall carbon nanotubes. *Carbon*. **49,** 2581 – 2602.

[16] Dresselhaus, M. S., Dresselhaus, G., Saito, R, and Jorio, A (2005). Raman Spectroscopy of Carbon nanotubes. *Physics Reports*. 50.

[17] Tessonier, J. P, and Su, D. S (2011). Recent Progress on Growth Mechanism of Carbon Nanotubes: A review. *ChemSuschem,* 0000, 00, 6-11

[18] Razali, M. H (2016). Physicochemical Properties of Carbon Nanotubes (CNTs) Synthesized at Low Temperature using simple Hydrothermal Method. *International Journal of Applied Chemistry.* **12** (**3**), 273 – 280.

[19] Trivedi, M. K, Tallapagada, R. M, Branton, A, Trivedi, D and Nayak G (2015). Characterization of Physical and Structural Properties of Aluminum Carbide Powder: Impact of Biofield Treatment. *J. Aeronaut Aerospace Eng*. **4** (**142**). 1000-1042

[20] Hou, Z., Wang, X., Ikeda, T., Terakura, K., Oshima, M and Kakimoto, M-A (2013). Electronic structure of N-doped graphene with native point defects. *Phys Rev B*. **87**: 165401.

[21] Hsieh, C. T and Teng, H (2002). Influence of oxygen treatment on electric double layer capacitance of activated carbon fabrics. Carbon. **40**: 667-674.

[22] Chen, J. H., Li, W. Z., Wang, D. Z., Yang, S. X., Wen, J.G and Ren, Z. F (2002). Electrochemical characterization of carbon nanotubes as electrode in electrochemical double-layer capacitors. *Carbon*. **40**, 1193 – 1197.

[23] Tansel, B., Sager, J., Rector, T., Garland, J., Strayer, R. F., Levine, L., Roberts, M., Hummerick, M and Bauer, J (2006). Significance of hydrated radius and hydration shells on ionic permeability during nanofilteration in deep end and cross flow modes. *Sep Purif Technol.* **51**: 40-47.